Emergent critical oscillations in motor cortex of Parkinson's patients

Short Title: Critical oscillations in Parkinson's disease.

Cheng Ly[1*], J. Sam Sooter[2], Andrea K. Barreiro[3], Woodrow L. Shew[2]

[1*]Mathematics Department, Virginia Commonwealth University, 1015 Floyd Ave, Richmond, 23284-2014, VA, U.S.A.
[2]Physics Department, University of Arkansas, 1 University of Arkansas, Fayetteville, 72701, AR, U.S.A.
[3]Mathematics Department, Southern Methodist University, P.O. Box 750156, Dallas, 75275-0156, TX, U.S.A.

*Corresponding author(s). E-mail(s): cly@vcu.edu;
Contributing authors: sooter@uark.edu; abarreiro@smu.edu; shew@uark.edu;

Abstract

The dynamical state of cortical neural activity constrains the complexity of functions it can perform. A marginally stable dynamical state - called criticality - is thought to be beneficial for brain functions that require multiple time scales, broad dynamic range, and large information storage and transmission. A growing body of evidence suggests that criticality is a feature of healthy brain dynamics, but breaks down in certain brain disorders. Here we ask whether Parkinson's disease incurs deviation from criticality compared to healthy controls. We analyze human resting state EEG activity in primary motor cortex. Parkinson's patients exhibit prominent oscillatory brain activity in multiple frequency bands (low delta and high theta) that is not present in controls. Surprisingly, we find that these emergent oscillations are close to criticality, i.e., amplitude fluctuations with approximate temporal scale invariance. We compare traditional signatures of criticality and more principled measurements of proximity to criticality using our new approach based on information theory and temporal renormalization group theory. Our new approach and traditional methods agree, demonstrating that critical dynamics are not always associated with healthy states; Parkinson's disease is associated with the emergence of near-critical oscillations in motor cortex.

Keywords: criticality, Parkinson's, EEG, motor cortex, temporal renormalization group, detrended fluctuation analysis

Author Summary

Brain function is thought to be optimal when its activity is near the border of order and chaos — a state called criticality. This state is thought to help the brain stay flexible and process information efficiently.

We investigate whether Parkinson's disease disrupts this balance like in other diseases and pathologies. Using resting EEG brain activity, we found that people with Parkinson's show strong rhythmic signals not seen in healthy brains, and surprisingly these rhythms are also near the critical state. Using both established and new theoretical tools, we show that critical dynamics can accompany disease, suggesting that being closer to criticality is not always a sign of healthy brain function.

Introduction

What are the properties of cortical neural activity that confer its ability to perform healthy functions? One long-standing hypothesis posits that a healthy brain operates in a dynamical state near *criticality* - a special, marginally stable state imbued with a wide range of scale-invariant time scales and optimal computation (Shew and Plenz, 2013; Hengen and Shew, 2025). Indeed, evidence for criticality is associated with improved cognitive performance in humans (Müller et al., 2025; Xin et al., 2025; Ezaki et al., 2020) and multiple beneficial computational properties including efficient coding (Safavi et al., 2024), large dynamic range (Kinouchi and Copelli, 2006; Shew et al., 2009; Gautam et al., 2015), discrimination of sensory input (Clawson et al., 2017; Gautam et al., 2015), and more. If these properties of criticality are needed for healthy brain function, it stands to reason that unhealthy dysfunction may be associated with deviation from criticality. This has indeed been reported in multiple studies (Zimmern, 2020). For instance, Alzheimer's disease (Montez et al., 2009; Ghassemkhani et al., 2025; McGregor et al., 2024), schizophrenia (Nikulin et al., 2012; Moran et al., 2019), depression (Linkenkaer-Hansen et al., 2005), and epilepsy (Fuscà et al., 2023) are associated with deviation from criticality compared to controls. However, the notion that healthy brain function requires closeness to criticality is challenged by some studies. For instance, sustained, focused attention seem to cause deviation from criticality (Irrmischer et al., 2018; Fagerholm et al., 2015). Here our primary goal was to determine how Parkinson's disease impacts criticality in motor cortex. Motor cortex is a crucial area for voluntary movement and muscle control, functions that are severely impaired in Parkinson's disease. We analyze a publicly available EEG dataset (Jackson et al., 2019; Swann et al., 2015; George et al., 2013) and ask whether motor cortex dynamics are closer to criticality for healthy control subjects or Parkinson's patients.

To rigorously measure proximity to criticality, we use our newly-developed approach based on information theory and Gaussian autoregressive processes that relies on developing temporal Renormalization Group (**tRG**) theory to find all of the critical points (Sooter et al., 2026). This approach measures distance from criticality (d_2) from time series data based on the nature of temporal fluctuations. We apply this framework to EEG data for the first time, to our knowledge, and compare it to traditional methods of quantifying timescales from time series (Zeraati et al., 2024) including the decay times of autocorrelation

function (**ACF**) (Müller and Meisel, 2023; Müller et al., 2025), and long-range temporal correlation via detrended fluctuation analysis (**DFA**) (Peng et al., 1994; Hardstone et al., 2012). However, we emphasize that our new approach rests on a mathematically rigorous definition of proximity to criticality, which is lacking in traditional methods (Tian et al., 2022).

We find that motor cortex resting state EEG activity in Parkinson's patients is marked by the emergence of near critical oscillations that are not present in healthy controls. Two recent studies are consistent with our results, although we measure distance to criticality directly. Calvo et al. (2024) found in whole-brain human MEG data that control subjects were further from a chaotic point in more frequency bands than Parkinson's, and Lee et al. (2024) found in whole-brain human EEG that control subjects had shorter timescales than Parkinson's in the theta band in some brain regions. Our results indicate that critical dynamics are not always associated with healthy states; Parkinson's disease seems to cause critical oscillations.

Results

How oscillations can be critical

A common notion about oscillatory time-series activity is that it cannot have critical dynamics because of the presence of a characteristic timescale (the period of oscillation). Because one feature of physical systems at criticality is the *absence* of a characteristic timescale, this would seem to be a contradiction.

An alternative question to ask, is whether the amplitude fluctuations of the oscillatory activity will display signatures of critical activity. This is referred to as *critical oscillations* (Palva and Palva, 2018). Neural activity within frequency bands is known to be relevant for neural computation (Buzsáki, 2006). In fact, using band-pass filtering and envelope extraction are general practice for large-spatial-scale time series data acquired through modalities such as EEG (Cohen, 2014) (see Fig 2A).

We show here that critical oscillations arise in a ground-truth model, and that the envelope fluctuations display the rich statistical properties associated with time series from critical systems. Because we have an analytically specified model, we can tune it closer to or further away from criticality; we also show that d_2 successfully identifies the proximity to criticality and is better than other common methods.

Consider a linear rate model, with population activity vector $\vec{x}(t)$ governed by:

$$\tau \frac{d\vec{x}}{dt} = A\vec{x} + \vec{\xi}(t) \tag{1}$$

where $x_j(t)$ is the activity of the jth neuron at time t, A is an $N \times N$ coupling (or adjacency) matrix with weights drawn from a Gaussian distribution with zero mean and variance of 2. Self-connections

were removed by setting all diagonal elements A_{ii} to zero. No additional structural constraints such as symmetry or Dale's law were imposed. $\vec{\xi}(t)$ is uncorrelated white noise: $\langle\vec{\xi}(t)\rangle = \vec{0}$, $\langle\xi_j(t)\xi_k(t')\rangle = \sigma^2\delta_{j,k}\delta(t-t')$; we set $N = 500$ and $\tau = 50\,\text{ms}$; we down-sampled the simulated activity to 46 ms time bins so it is comparable to data (Pachitariu et al., 2025). This model has been widely used and insightful for studying critical dynamics, for example by Hu and Sompolinsky (2022); Dahmen et al. (2019) who derived formulas for the spectrum of the covariance (and studied dynamics near criticality with applications to experimental data), Morales et al. (2023) used this model framework to infer the spectrum paired with phenomenological renormalization group applied to experimental data to compare scale-invariant statistics from recordings across many different brain regions, and most recently by Fontenele et al. (2026) to study hidden critical modes.

The spectrum of A determines whether this model exhibits critical dynamics, i.e., $\max Re(\lambda) = 1$ corresponds to criticality, where λ are the eigenvalues of A. More generally, if $Re(\lambda_i) = 1$, then the ith mode is at criticality, and furthermore if $Im(\lambda_i) \neq 0$ then the ith mode will display critical oscillations (Fontenele et al., 2026). Below we demonstrate: i) how critical oscillations can emerge, ii) our distance to criticality method d_2 (measured in bits/sec to quantify accumulation of evidence for ruling out being at criticality, see **Methods: Temporal renormalization group theory**) applied to the entire population averaged activity in the model $\nu(t) := \frac{1}{N}\sum_j x_j(t)$, with band-pass filtering and envelope extraction, is an excellent approximation to the ground truth assessment of proximity to criticality, iii) other methods (autocorrelation function (**ACF**) timescale, detrended fluctuation analysis (**DFA**); see Fig 1C and **Methods**) behave as expected at criticality even with prominent oscillations.

Our model study of proximity to criticality involves scaling all entries of the coupling matrix A so that $\max Re(\lambda) \to 1^-$ (Fig 1A), which leads to rich network activity statistics (Fontenele et al., 2026). The power spectrum of the entire population averaged activity $\nu(t)$, i.e, PSTH, has a prominent peak as the network approaches criticality (Fig 1B), i.e., critical oscillations. This behavior is easily constructed by insuring the leading eigenvalue ($\max Re(\lambda)$) is complex and has non-zero imaginary part; the power spectrum has a prominent peak because of the leading oscillatory mode even though there are contributions from other non-oscillatory modes. We apply our distance to criticality method to the PSTH $\nu(t)$ of the entire population after band-pass filtering and envelope extraction, akin to what we will do in the EEG data. Figure 1D–F shows that it well-approximates the ground truth distance to criticality d_2 in the model. A consequence of (near) critical dynamics is that traditional measures for assessing lengths of timescales should diverge, which is precisely what we observe in the model with ACF timescale (the first time the ACF crosses below a threshold, Fig 1E); also, the DFA exponent increases

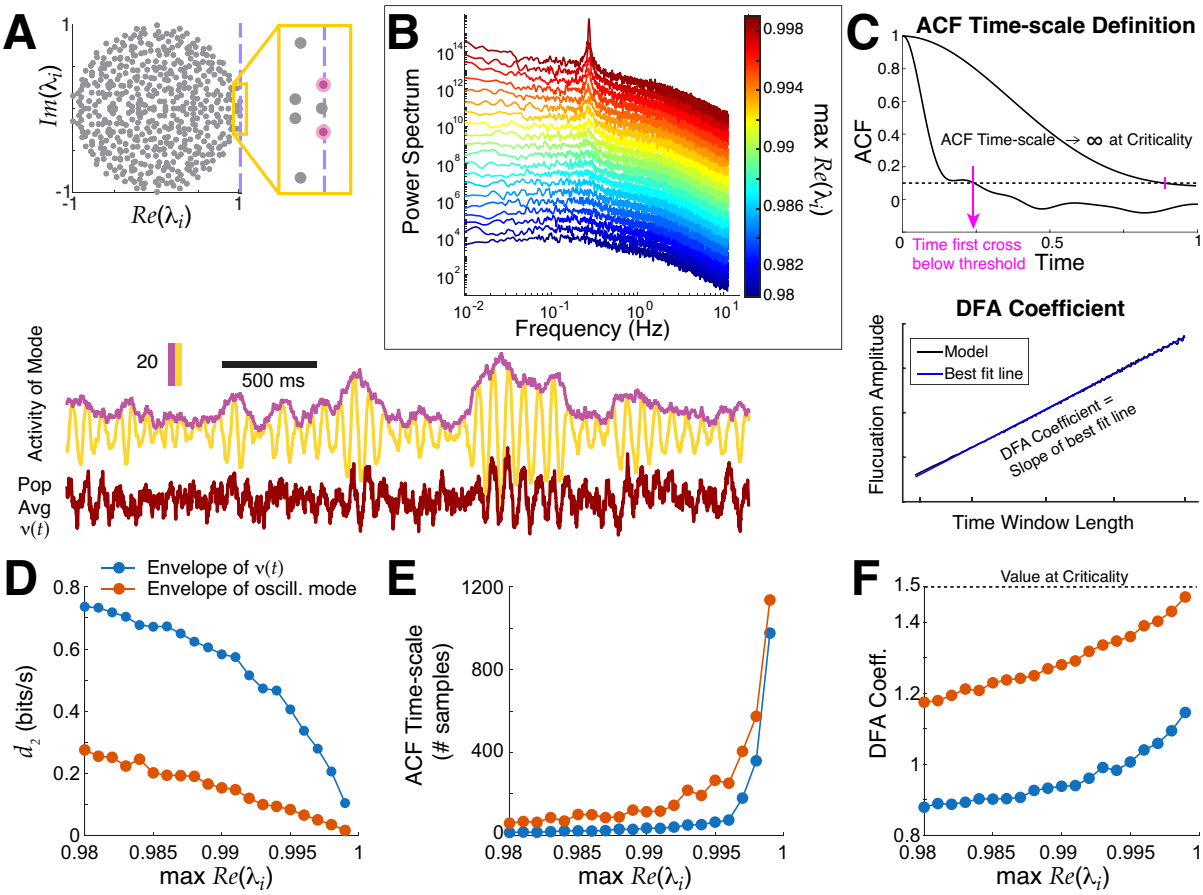

Fig. 1 Critical oscillations in a ground truth model are well-captured by our methods. A) Top: spectrum of coupling matrix A near critical oscillations. Bottom: simple population average $\nu(t)$ (dark red bottom trace) does not have critical dynamics but the oscillatory mode (yellow) has critical dynamics in the amplitude fluctuations, revealed by taking the envelope (purple). **B)** The power spectrum of $\nu(t)$ as the network approaches criticality has emergent oscillations (blue to red). **C)** Two traditional methods for measuring time-series data: ACF timescale (top) and DFA (bottom, no numbers/units for demo). A consequence of approaching critical dynamics is ACF timescale increases and DFA coefficient approaches 1.5. **D, E, F)** Our distance to criticality method d_2, ACF timescale (number of samples; $\nu(t)$ was down-sampled to 46 ms time bins (Pachitariu et al., 2025)), and DFA coefficient calculations applied to $\nu(t)$ (blue) all well-approximate the underlying critical oscillations (blood orange) that are obscured in the entire population activity.

(Fig 1F). Finally, the network activity $\nu(t)$ also exhibits avalanche statistics when very close to criticality (Fig 2 in (Fontenele et al., 2026)).

We also observe that in this model, taking the whole population average obscures the presence of critical oscillations in the leading mode (blue curves are not the same as the blood orange curves in Fig 1D–F), but nevertheless these methods applied to the whole population monotonically track the ground truth.

Taken together and considering that d_2 is a rigorous and direct measure for distance to criticality, we conclude that using d_2 is a better measure for quantifying critical oscillations in real data given that the ground truth is inaccessible. Having validated the use of distance to criticality in a model where the ground truth is known, we next applied the method to an EEG dataset.

Application to EEG Parkinson's data

We use freely available resting state EEG data (Fig 2A) collected by a lab in UCSD (Jackson et al., 2019; Swann et al., 2015; George et al., 2013) using a standardized format (Pernet et al., 2019; Appelhoff et al., 2019). Following previous studies (Jackson et al., 2019; Swann et al., 2015), we analyze data from the two electrodes positioned over left and right primary motor cortex (**M1**) labeled C3 and C4 (Fig 2A), an important brain region for motor planning and voluntary movement, functions that are impaired in these Parkinson's patients. The dataset consists of 3 minute recording sessions from 16 healhty control subjects (**control**) and 15 subjects with Parkinson's disease in two states: off drugs and on drugs to manage their symptoms. The Parkinson's patients exhibited slight variability in severity of the disease as measured by Unified Parkinson's Disease Rating Scale (**UPDRS**) III, but otherwise were not cognitively impaired compared to control subjects via Mini-Mental Status Exam (**MMSE**) or the North American Reading Test (**NAART**) (George et al., 2013). We use a common approach of applying a band-pass filter to the EEG data and subsequently extracted the amplitude envelope (Cohen, 2014) (Fig 2A right panel) to be used as the signal for all the analyses here (except Fig 2B). By studying fluctuations of the amplitude envelope, we can assess whether the oscillations at particular frequency bands are near or far from criticality. By definition a critical oscillation will have amplitude fluctuations that are temporally scale invariant (Fontenele et al., 2026; Palva and Palva, 2018). This approach follows the long tradition of studying critical oscillations, typically referred to as long range temporal correlations (**LRTC**) (Linkenkaer-Hansen et al., 2001, 2005; Jackson et al., 2019; Hohlefeld et al., 2012, 2015), an entity that is known to increase with critical dynamics.

This EEG data has power in select frequency bands (Fig 2B), a common observation in other resting state EEG data (Newson and Thiagarajan, 2019). Importantly, the timescales and dynamics in the broadband signal (Fig 2B) are distinct from the corresponding entities in band-passed power-envelope signal that is the main focus of our study. Figure 2B shows the population average (across 16 control subjects and 15 Parkinson's patients) power spectrum of the envelope of the EEG data (y-axes on a log-scale) without band-pass filtering. Whether considering the average of both C3 and C4 (left panel), or a single electrode alone (C3 in middle, C4 in right panel), it is evident that control subjects on average (black curve) have peaks in their power spectrum in the upper theta-band (4 to 8 Hz) to lower alpha-band (8 to 13 Hz). Parkinson's patients exhibit similar power spectra to controls, except for the emergence of oscillations in the lower δ-band (1 to 4 Hz) for patients off medication and upper θ- to α-bands for all patients.

First, we analyze the timescales of fluctuations in oscillation amplitudes using two traditional tools: autocorrelation (see Fig 3A and Eq (2)), detrended fluctuation analysis (see Fig 4A and **Methods:**

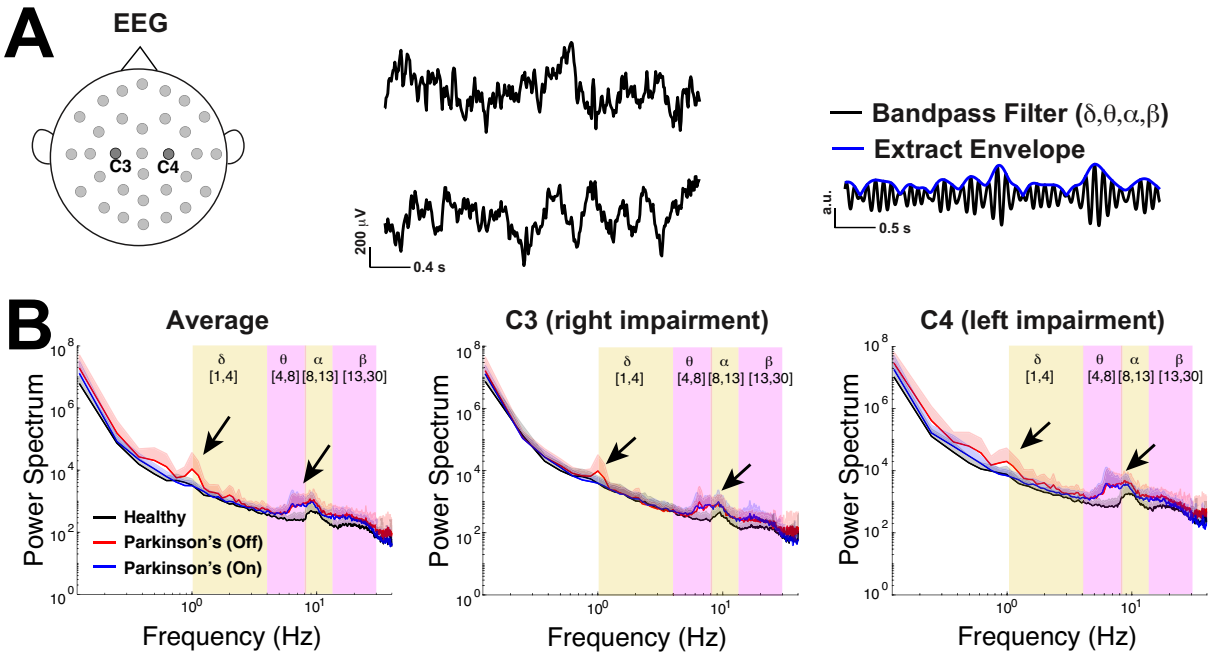

Fig. 2 Emergent δ and θ oscillations in Parkinson's patients. A) EEG time-series from two electrodes at the primary motor cortex on the left (C3) and right side (C4); right panel illustrates extracting the envelope of the band-passed EEG recording. **B**) The population-averaged power spectrum of the envelope of the EEG (without any band-pass filtering) for respectively the average of C3 and C4, as well as C3 and C4 individually, all exhibit peaks in the lower delta-band for Parkinson's patients off medication (red), peaks in upper theta- to lower alpha-bands for Parkinson's patients (on and off drugs), and a peak in the alpha-band for control (black). The shaded region above the curve corresponds to one standard deviation across the subjects.

Detrended Fluctuation Analysis). Then, we compare to our new information theoretic method for measuring distance to criticality d_2, (where tRG theory was used to find all of the scale-invariant fixed points) that goes beyond simple measures of timescales. For the control subjects, we simply use the average of both electrodes, but for Parkinson's patients we use the electrode that corresponds to the side that subjects are reported to have physical limitations, see Table 3. (The results reported in the main text (Figs 3–5) also hold when we use both electrodes in Parkinson's patients, see Supplementary Text S1 and Figures S1, S2.) Figure 3A shows the average autocorrelation function (over the number of subjects) in the four frequency bands (the alpha- and theta- bands zoomed-in to the right of the main axes) where the control subjects (black curves) have consistently faster decay than Parkinson's patients (blue and red, x-axis at specific time lags is a log-scale). As in the earlier plot (Fig 1C,E) we calculate the 'ACF timescale' by finding the first time a subject's ACF falls below a chosen threshold (Fig 3B). The population ACF timescales exhibit statistically significant differences between healthy control and Parkinson's patients, specifically the control subjects generally have faster timescales than Parkinson's patients (both on and off drugs) in the delta- and theta- frequency bands (population summarized with box plots, Fig 3C), statistical significance was assessed with the Wilcoxon rank-sum test (see **Methods: Wilcoxon Rank-Sum Test** for details). When the differences were significant, the effect sizes are medium to large (see Table 1). There are no statistical differences between Parkinson's patients on drugs

versus off drugs (see Table 1; the population means are included in Fig 3D for completeness). Although commonly used, the autocorrelation function simply measures statistical correlation at a specific time lag averaged over the entire time series, in contrast to other measures that account for fluctuation trends as window sizes vary (DFA). Note that there are other methods for extracting timescales from the ACF, such as fitting an exponential function (Siegle et al., 2021; Li and Wang, 2022; Zeraati et al., 2022, 2024) or its variants (Zeraati et al., 2022; van Meegen and van Albada, 2021); but in this data, neither the population averages nor individual ACFs are well-fit exponential functions.

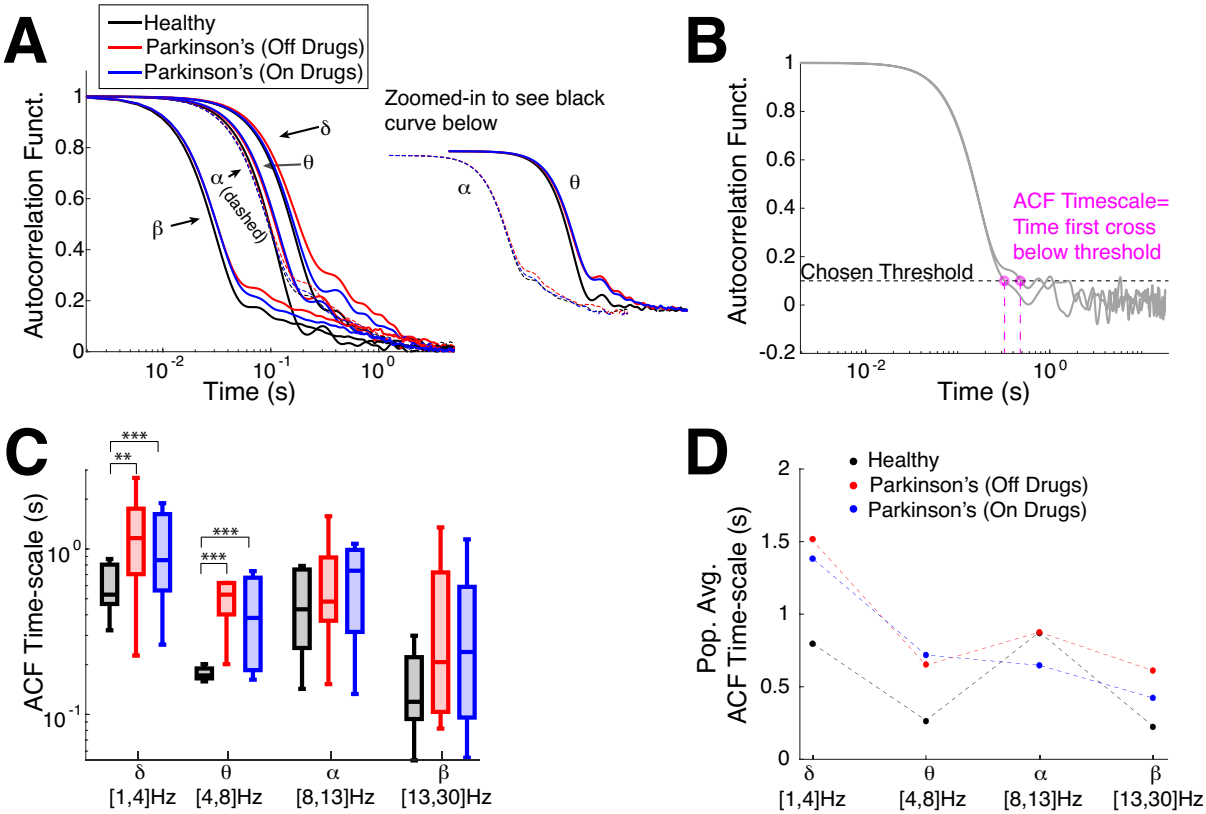

Fig. 3 Emergent Parkinson's oscillations have large autocorrelation time. A) The population-averaged ACF in Parkinson's patients has longer timescales (red, blue: slower decay) in motor cortex EEG activity across all 4 frequency bands than healthy (control). ACF in alpha- and theta-band are zoomed-in and shifted for clarity. **B)** Example calculation of ACF timescale, i.e., a measure of ACF decay time, for 2 subjects; the first time where a subject's ACF falls below a chosen threshold of 0.1. **C)** Summary of ACF timescale with box plots in different frequency bands shows that control subjects on average have faster ACF time decay (smaller timescale) than Parkinson's patients for the lower frequency bands (delta and theta). The horizontal lines in the boxes represent inter-quartiles: 25th percentile, median, and 75th percentile. Difference in distributions are statistically significant measured by Wilcoxon rank-sum test (see Table 1 for details). **D)** The population means of ACF timescale are plotted for completeness.

Next we perform DFA analysis, which characterizes how fluctuations vary across different timescales, also known as long range temporal correlation (**LRTC**). In the DFA analysis we find that control subjects have on average shorter range temporal correlation than Parkinson's patients, consistent with the lower frequency bands in the ACF timescale analysis. A demonstration of the DFA method is depicted in Figure 4A on a control subject's resting state EEG in the delta-band where the fluctuation amplitude

Table 1 Statistics to show that control subjects have shorter time scales than Parkinson's using ACF timescale measure; see Figure 3C. Using Wilcoxon rank-sum test where the null hypothesis is that both data samples are drawn from the same distribution. Top shows $p-$values, bottom shows effect size (see **Methods: Wilcoxon Rank-Sum Test**).

Relationship / $p-$value	δ band	θ band	α band	β band
Cntrl. vs. Park. (Off drugs)	1.5×10^{-2}	4.6×10^{-5}	0.33	0.18
Cntrl. vs. Park. (On drugs)	6.6×10^{-2}	2.2×10^{-3}	0.42	0.24
(Park.) On vs. Off	0.43	0.27	0.91	0.88

Relationship / Effect Size	δ band	θ band	α band	β band
Cntrl. vs. Park. (Off drugs)	0.44 (med)	0.73 (lrg)	0.41 (n/a)	0.24 (n/a)
Cntrl. vs. Park. (On drugs)	0.33 (med)	0.55 (lrg)	0.15 (n/a)	0.21 (n/a)
(Park.) On vs. Off	0.14 (n/a)	0.13 (n/a)	2.3×10^{-2} (n/a)	2.7×10^{-2} (n/a)

as a function of time window length in log-log coordinates requires 2 lines at a dividing point; such a dividing point is required in about 72% to 85% of the time (counting all frequency bands, subject type, and electrode combinations). In such cases, we use the slope of the best fit line for larger time windows (second segment to the right), and call this the DFA coefficient. When there are no temporal correlations (i.e., white noise) the DFA coefficient is 0.5. In a random walk, temporal memory is infinite and the DFA coefficient is 1.5. DFA coefficients between 0.5 and 1.5 indicate intermediate temporal correlations. A summary of all DFA coefficients is shown with box plots in Fig 4B with four frequency bands: on average control subjects have a much shorter range of temporal correlation, i.e., timescales, than Parkinson's patients (on or off drugs). The trend that control subjects have shorter timescales than Parkinson's patients is robust across all four frequency bands we consider, with the alpha-band results having comparatively weaker results with larger $p-$values using Wilcoxon rank-sum test. The DFA coefficients shown include all 16 control subjects, but for Parkinson's 1 or 2 patients were excluded (depending on frequency band) because the fluctuation amplitudes for a few subjects were too variable to be well fit by a line (see Fig S3 and Supplementary Text S1). Figure 4C clearly demonstrates how different the population averages are; control subjects have much smaller average DFA coefficients than Parkinson's, and Parkinson's patients have similar DFA coefficients regardless of whether on or off drug treatments.

Table 2 Statistics to show that control subjects have shorter time scales than Parkinson's using DFA coefficient; see Figure 4B. Using Wilcoxon rank-sum test where the null hypothesis is that both data samples are drawn from the same distribution. Top shows $p-$values, bottom shows effect size (see **Methods: Wilcoxon Rank-Sum Test**).

Relationship / $p-$value	δ band	θ band	α band	β band
Cntrl. vs. Park. (Off drugs)	9.4×10^{-3}	9.4×10^{-3}	8.6×10^{-2}	2.8×10^{-2}
Cntrl. vs. Park. (On drugs)	7.7×10^{-2}	5.7×10^{-3}	2.4×10^{-2}	9.1×10^{-3}
(Park.) On vs. Off	0.28	0.51	0.89	0.96

Relationship / Effect Size	δ band	θ band	α band	β band
Cntrl. vs. Park. (Off drugs)	0.47 (med)	0.47 (med)	0.31 (med)	0.11 (sm)
Cntrl. vs. Park. (On drugs)	0.32 (med)	0.51 (lrg)	0.42 (med)	0.14 (sm)
(Park.) On vs. Off	0.2 (n/a)	0.13 (n/a)	0.26 (n/a)	1.5×10^{-3} (n/a)

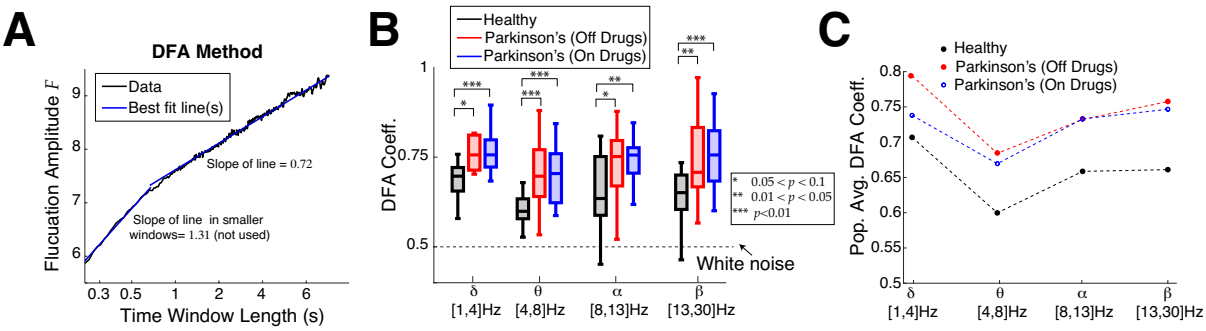

Fig. 4 Emergent Parkinson's oscillations have larger DFA exponents. A) Example DFA coefficient calculation (control subject 1 in delta-band) well-fit with 2 line segments, where a choice for the time window to use has to be made. When 2 lines are used, the slope of the right line segment for larger time windows is reported. **B)** Summary of DFA coefficients with box plots in different frequency bands is largely consistent with the ACF results (Fig 3C,D). Box plot convention are the same as in Figure 3C. The results are not as strong in the alpha-band. Difference in distributions are statistically significant measured by Wilcoxon rank-sum test (see Table 2 for details). **C)** The population means of DFA coefficients are plotted to clearly illustrate that control subjects are further from criticality/scale-invariance than Parkinson's patients.

Although both ACF and DFA results provide evidence that control subjects' EEG motor cortex activity is further from criticality than Parkinson's patients, these analyses do not directly measure distance to criticality. To this end, we developed a rigorous tRG theory and implemented pragmatic computational tools to directly calculate distance to criticality (d_2). The d_2 measure has several specific advantages : i) unlike DFA, it does not require specifically choosing a time window segment and assessing quality of linear fits (Fig S3), ii) unlike ACF, it does not require a prescribed threshold to find timescale, iii) the distance to criticality d_2 (Fig 5A) is a precise quantification of distance independent of model parameterization, calculated in units of bits/sec (measure of evidence for ruling out being at criticality). Our framework requires first fitting an auto-regressive (AR) model to the data, then calculating the distance of the fitted model to the critical state; see **Methods: Temporal Renormalization Group Theory** and Figs S5–S7 for further details.

We perform a detailed comparison of Parkinson's and control subjects using d_2 and find control subjects' EEG in primary motor cortex are generally further from criticality than Parkinson's patients. We specifically vary the AR model order (16 to 24) as well as the time bin length (2 ms up to 100 ms) – we previously showed that increasing the time bin can unveil critical dynamics (Fontenele et al., 2024) and that d_2 is expected to decrease monotonically with increasing model order and with increasing time bin length (Sooter et al., 2026). Figure 5B shows, within a given subject group (healthy, Parkinson's on/off drugs) for a fixed AR model order 20, that d_2 tends to decrease as time bin length increases, except occasionally in the delta-band (light blue), and that there are minor differences in population d_2 across frequency bands with a given time bin. Varying AR model order and time bin length simultaneously results in a wide variety of '**temporal reach**' (x-axis of Fig 5C,D) defined as the the AR model order multiplied by the specific time bin, i.e., the maximal time in the past that can influence present AR model value. The temporal reach values we consider have a large range from 32 ms to 2.4 s. The population

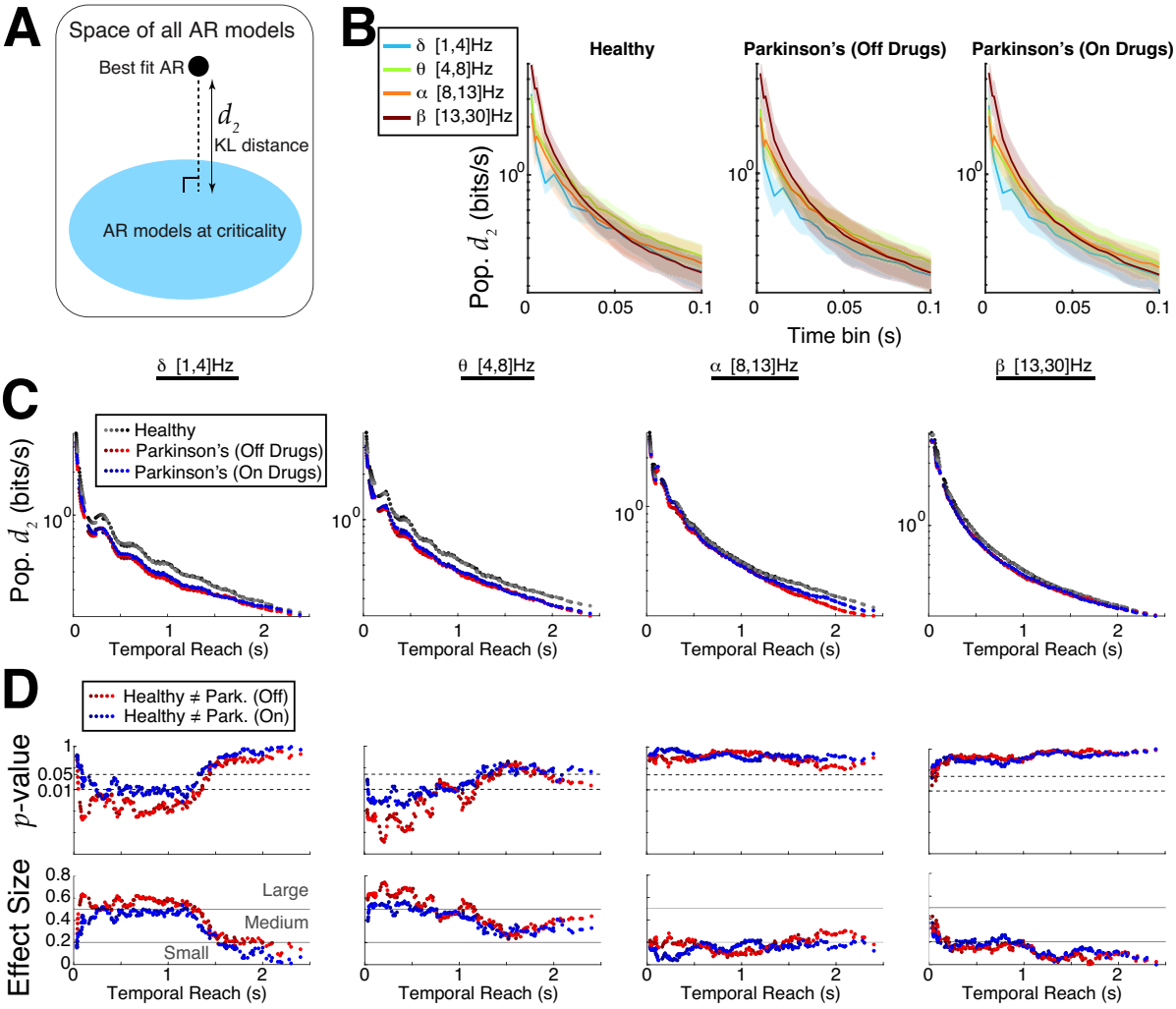

Fig. 5 Emergent Parkinson's oscillations are closer to criticality. A) Using new theory to quantify differences in distance to criticality between controls and Parkinson's patients after data is fit with an AR model. **B)** The population d_2 (bits/s) values (log-scale) grouped by control and two Parkinson's state as a function of coarse-grained time bin with AR model order 20 shows little difference across different band-passed frequencies. **C)** Summary of population d_2 values (log-scale) for many time bins and model orders; the x-axis represents the 'temporal reach', i.e., model order multiplied by time bin length (varies from 2 ms to 100 ms). The control subjects consistently had larger d_2 and were thus further from criticality than Parkinson's patients, independent of model order, time bin length, or frequency band. **D)** Quantifying the statistical significance of our results using Wilcoxon rank-sum test, showing the $p-$values (log-scale) and effect sizes (see **Methods: Wilcoxon Rank-Sum Test**). The different shades of colors in C) and D) correspond to AR model fits of different orders ranging from 16 to 24.

averaged d_2 for many temporal reach values is shown in Figure 5C (y-axis is log-scale, different color shades correspond to different AR model order), where it is evident that Parkinson's patients (red and blue dots) are closer to criticality (d_2 below) than controls (black/gray) in the delta- and theta-bands. We use Wilcoxon rank-sum test to analyze whether differences between Parkinson's and control are statistically significant under the null hypothesis that the values were generated from the same probability distribution ($p-$values in top row of Fig 5D). The differences are clear in the delta- and theta-bands for a wide range of temporal reach values, there is no differences in the alpha band, and differences in the beta-band are only evident with small temporal reach values. The effect size and a qualitative characterization

of effect size (small, medium, large (Cohen, 2013; Tomczak and Tomczak, 2014)) is shown in the bottom row of Figure 5D.

Discussion

Here we have shown that the prominent δ and θ band oscillations that emerge in Parkinson's disease from EEG motor cortex are, in fact, near-critical oscillations. Although each of these oscillations is defined by particular timescales (the oscillation periods), the power (amplitude) of these oscillations exhibits fluctuations across a wide range of time scales. These amplitude fluctuations are approximately scale invariant, which is how critical oscillations are defined (Fontenele et al., 2026; Palva and Palva, 2018). In contrast, in healthy controls, the same frequency bands have amplitude fluctuations that are further from criticality.

The distance measure d_2 enables a fair comparison of different time series, and is a rigorous information-theoretic entity in units of bits/s that measures the amount of evidence for ruling out the hypothesis that the data are at criticality (Sooter et al., 2026). Although the ACF and DFA analyses yielded similar results, d_2 is a direct measure for distance to temporal scale-invariance, and proved to be cleaner for delineating differences (control vs. Parkinson's), and did not require making specific choices regarding threshold cut-offs, which time window segments to use, etc. Unlike traditional methods, the analysis with d_2 goes beyond just measuring timescales, and also clearly shows how the differences depend on the 'temporal reach', and that distances to criticality tend to decrease with increasing temporal reach. For both DFA and d_2, the strongest separation between control and Parkinson's patients are in the delta- and theta-bands, followed by the beta-band, with the weakest results in the alpha-band. The ACF timescales only had significant differences in the delta- and theta- band. The relative consistency of these results suggests that there are real and surprising differences between control and Parkinson's patients in motor cortex EEG.

Our results in motor cortex are at odds with the idea that, in general, healthy brains operate closer to criticality than pathological ones (Hengen and Shew, 2025; O'Byrne and Jerbi, 2022), as discussed in the Introduction. However, our results are in line with two recent publications where it was reported that Parkinson's patients i) have more frequency bands closer to 'edge of chaos' (a point related to criticality) than control subjects in whole brain MEG (Calvo et al., 2024), and ii) can have longer timescales as measured with DFA coefficients in whole brain EEG in the theta-band (Lee et al., 2024). These studies are different than ours because they focused on whole brain imaging and included many more subjects with which they aggregated/averaged. The number of subjects we used enabled detailed analysis, for example to assess the quality of model fits for each subject.

Along these lines, another recent study showed that a measure of 'intrinsic neural timescale' using fMRI was longer in late stage Parkinson's patients than in healthy controls in the anterior cortical region (Wei et al., 2024). This study is in line with our results, but unlike our d_2, their measure of intrinsic neural timescale is indirect because it involves calculating when various ACFs first cross below a threshold, smoothing the maximum of those values over space and applying a z-transform. The timescales of fMRI measurements are coarser than those of EEG, with temporal resolution on the order of seconds, so we cannot make any direct comparisons with our results.

Interestingly, Parkinson patients on versus off drugs to treat motor symptoms did not ever have statistically significant differences in their motor cortex EEG, independent of the methods (ACF, DFA, d_2). Presumably, these drugs helped mitigate their motor symptoms to some extent, but the motor cortex activity that is responsible for voluntary movement planning and muscle control did not exhibit any changes in timescales in the resting state. Perhaps EEG amplitude fluctuations in motor cortex in the resting state are not a direct reflection of mitigated motor symptoms with medication, but rather indicate the difference between Parkinson's disease itself compared to control.

Methods

Ethics statement

This article presents an accurate account of the work performed by the stated authors, and all underlying data are represented accurately with consent from the owners. To the best of our knowledge, this work is original and is not under consideration for publication elsewhere. The study used publicly available data with accurate citation, and all methods were performed in accordance with relevant guidelines and regulations. The authors declare no conflicts of interest related to this research.

This study uses third party human EEG data that is publicly available (George et al., 2013; Swann et al., 2015; Jackson et al., 2019) (see Data and code availability section). The Materials and methods section in their papers explicitly state that 'All the participants provided written informed consent according to an Institutional Review Board Protocol at the University of California, San Diego and the Declaration of Helsinki'. We have also obtained written approval from the authors to use their data in this study.

Parkinson's patient characteristics

Table 3 shows side of physical impairment in the Parkinson's patients.

Table 3 The side of reported physical impairment in Parkinson's patients (Appelhoff et al., 2019; Rockhill et al., 2021) and thus corresponding electrode used. Electrode C3 is on the left motor cortex, C4 on the right motor cortex. Note that all subjects had the same side for physical impairment on and off drug treatment except for subject 14 who switched to Right side (C3) while on drug treatment.

Subject	Impairment Side	Electrode
1	Right	C3
2	Both	Both
3	Right	C3
4	Right	C3
5	Left	C4
6	Right	C3
7	Left	C4
8	Left	C4
9	Left	C4
10	Right	C3
11	Right	C3
12	Right	C3
13	Left	C4
14	Left*	C4*
15	Right	C3

Autocorrelation function

The autocorrelation function is a common tool used to characterize how related (correlated) a time series of data $x(t)$ is with specific time lags τ. The autocovariance function of a time series $x(t)$ is:

$$\tilde{A}(\tau) := \mathbb{E}_t[x(t)x(t+\tau)] - \Big(\mathbb{E}_t[x(t)]\Big)^2, \tag{2}$$

and the autocorrelation function is simply:

$$A(\tau) = \tilde{A}(\tau)/\sigma_X^2 \tag{3}$$

where $\sigma_X^2 := \mathbb{E}_t\left[\big(x(t) - \mu_X\big)^2\right]$ is the point-wise variance of the time series. We calculate the autocorrelation function of a particular time series of EEG via the Matlab function `autocorr` on centered data $x(t) - \mathbb{E}_t[x(t)]$ with 10,000 lags (recall the time bins are 2 ms) and 1.96 standard deviations: `autocorr(X-mean(X),'NumLags',10000,'NumStd',1.96)`. The results are in Figures 3, S1.

Detrended Fluctuation Analysis (DFA)

DFA is a common method for quantifying the degree of long-range temporal correlations (Peng et al., 1994). For a given time-series, the DFA coefficient was calculated by assessing the correlation of fluctuation amplitudes in various time window lengths. Start with a time-series x_j, then calculate the

cumulative sum: $Y_t := \sum_{j=1}^{t} x_j$. The 'entire' Y_t time-series is divided into n equal lengths for the duration of the specified time window τ_x of length $(\tau_x/dt + 1)$ – if the length of Y_t cannot be evenly divided, the end of the time-series is truncated, so $n = \lfloor N/(\tau_x/dt + 1) \rfloor$. Then for each segment of length $(\tau_x/dt + 1)$ the *local trend* (least squares linear fit L_k) is calculated. After which the mean-squared deviation is calculated: $G(n,i) = \frac{1}{n} \sum_{t=(i-1)n+1}^{(i-1)n+n} (Y_t - L_k(t))^2$, then the mean fluctuation amplitude is: $F(n) = \sqrt{\frac{1}{\lfloor N/n \rfloor} \sum_{i=1}^{\lfloor N/n \rfloor} G(n,i)}$. Finally, the least squares linear fit between $\log(n)$ (horizontal axis) and $\log(F(n))$ (vertical axis) is calculated – the slope of this line is called the *DFA coefficient*.

In cases where $\log(n)$ versus $\log(F(n))$ is not well-fit by a single line, the time windows are split in two segments determined manually, then two least squares linear fits are calculated with the larger windows (right half) determining the DFA coefficient (Gu et al., 2015).

Temporal renormalization group (tRG) theory

A system is at criticality if (1) it lies at a boundary between qualitatively different operating regimes and (2) it exhibits scale-invariance, i.e. the lack of a characteristic spatial or temporal scale (Hengen and Shew, 2025). The renormalization group (**RG**), which was originally developed to study critical phenomena in condensed matter systems, brings mathematical precision to these statements. The core idea of RG is to gradually remove the fine-scale details of a model to generate new, effective models at coarser scales. Fixed points of the RG operation therefore correspond to models that are scale-invariant, and all of the models in the basin of attraction of such a fixed point share the same coarse-scale behavior - this is the fundamental reason why, for example, water and ferromagnets poised near their respective phase transitions have quantitatively identical scaling exponents despite their drastic dissimilarities at microscopic length scales. Some RG fixed points are stable, meaning that there is an extended region in model space surrounding the fixed point such that every model in the region flows into the fixed point. Such fixed points fail to satisfy condition (1) in the definition of criticality. (For example, the RG fixed point corresponding to the disordered phase of an Ising model is stable.) Models lying in the basins of attraction of *unstable* fixed points, on the other hand, are both scale-invariant and poised at a boundary between different operating regimes, and hence are at criticality.

In traditional applications of RG to spatially organized systems (e.g. Ising-type models), coarse-graining is implemented in space. Neural systems, on the other hand, can have rich temporal dynamics in an measurable entity (i.e., population EEG) independent of whether there is weak or crucial spatial structure. In Sooter et al. (2026), we argued that the appropriate way to define criticality in such systems is with a temporal RG (**tRG**), wherein high-frequency features of a model are gradually removed to

reveal its asymptotic behavior at low frequencies. We applied this procedure to a fundamental class of univariate discrete-time stochastic dynamical systems, Gaussian autoregressive (**AR**) models:

$$x_t = \sum_{j=1}^{n} \phi_j x_{t-j} + \xi_t. \tag{4}$$

We chose AR models both because they are analytically tractable, and because they are the optimal choice in a precise *max ent* sense. Specifically, if an observed time series is short enough that we can only confidently estimate its second-order (autocovariance) statistics, then AR models are the maximum entropy (i.e. minimally presumptive) way to model those statistics (Choi and Cover, 1984). In an AR model, the state x_t at time t is a linear, Gaussian readout of the recent history (up to some maximum lag n, called the model order):

$$x_t \sim \mathcal{N}\left(\sum_{k=1}^{n} \phi_k x_{t-k}, \sigma^2\right).$$

In the space of order-n AR models, there are $n+1$ tRG fixed points, which we can label using the power-law exponents of their respective power spectra, $\beta = 0, 2, \ldots, 2n$. The $\beta = 0$ fixed point is stable and corresponds to white noise - this is the "trivial" fixed point that any AR model with a finite characteristic timescale flows into. The basins of attraction of the $\beta \geq 2$ fixed points constitute the AR models that are at criticality.

Next, we asked how we should quantify proximity to these basins. That is, having determined which AR models are *at* criticality, can we say which ones are *close* to criticality? Naively, we could measure the Euclidean distance (in the parameter space defined by the AR model history kernel ϕ) from an AR model to each of the basins of attraction. However, there is no principled reason to use Euclidean distance rather than some other metric. To resolve this ambiguity, we turned to information theory and *define* proximity to criticality as distinguishability (per unit time) from a system at criticality. Specifically, for a given order-n AR model B, let:

$$d_\beta(B) := \inf_{A \in A_\beta^{(n)}} \lim_{T \to \infty} \frac{1}{T} KL\left(P_B(x_1, \ldots, x_T) || P_A(x_1, \ldots, x_T)\right) \tag{5}$$

where $A_\beta^{(n)}$ is the set of order-n AR models that flow into the β fixed point, $P_A(x_1, \ldots, x_T)$ is the probability distribution for a $T-$step draw from the AR model A (and similarly for P_B), and $KL(\cdot||\cdot)$ is the Kullback-Leibler divergence. The structure of basins of attraction is such that that infimum taken over the set of all critical models $\cup_{\beta \geq 2} A_\beta^{(n)}$ is equal to the infimum taken over the $\beta = 2$ basin of attraction (Sooter et al., 2026); hence we only report d_2 in this paper.

To estimate d_2 from EEG data after bandpass filtering and extracting the envelope, we: 1) fit an AR model to the data using the Yule-Walker method, and 2) compute d_2 for this model using Eq (5).

Wilcoxon Rank-Sum Test

We use the Wilcoxon rank-sum test (**WRST**) because it is ideal for the EEG. It is a nonparametric test of the null hypothesis that two groups of data are generated from the same distribution. The $p-$values of this test correspond to the probability that the null hypothesis holds. In addition, we report the *Effect Size* of the WRST:

$$\text{Effect Size} := \frac{|z|}{\sqrt{n_1 + n_2}} \tag{6}$$

where z is the $z-$score of the $U-$statistic, $z = (U - \mu_U)/\sigma_U$ and n_j are the sample sizes for the two populations. Effect sizes for $t-$test and Wilcoxon rank-sum test with values: $(0, 0.2]$ are considered **small**, $(0.2, 0.5]$ are **medium**, $(0.5, 0.8]$ and above are **large** (Cohen, 2013; Tomczak and Tomczak, 2014); these labels are simply a qualitative assessment.

EEG Data

We used freely available EEG collected years ago that have appeared in many studies (Jackson et al., 2019; Swann et al., 2015; George et al., 2013) and was made widely applicable following common standards (Pernet et al., 2019; Appelhoff et al., 2019). We used all 16 control (control) subjects and all 15 Parkinson's patients except for some of the DFA coefficients (see Figure S3). We used an EEG reader function by Tcheslavski (2025).

Frequency Band Limits

The frequency bands of interest were limited with an upper bound in the beta band (30 Hz) because the 60 Hz grounding frequency (inferred by the power spectrum of all electrodes have a large peak at 60 Hz); any signals close to 60 Hz are considered artifacts perhaps due to electrical interference. For completeness and since some EEG studies report results in the gamma band frequency (George et al., 2013; Swann et al., 2015), we repeated our analysis on a lower gamma band frequency between 30 and 50 Hz (as was done in George et al. (2013), and found that the general trend of results we observed did not hold (see Fig S4, except for the population averaged ACF decay Fig S4A). We note however that in this lower gamma frequency band, the DFA analysis was messier than the other 4 lower frequency bands; in particular for the control subjects where 5 were excluded (see GitHub page), and in one of the ACF timescales was unusually long (longer than 20 s). Thus, these results should be taken with caution.

Data and code availability

Declarations

Data availability. The raw EEG dataset was collected at UC San Diego from a team of researchers, it is freely available (Rockhill et al., 2021) at https://openneuro.org/datasets/ds002778/versions/1.0.2.

Code availability. See https://github.com/chengly70/parkeeg for MATLAB code implementing all computational components in this paper.

Author Contributions. Conceptualization: CL, WLS. Methodology: CL, JSS, WLS. Sofware: JSS, CL. Validation: CL. Formal Analysis: CL. Investigation: JSS, CL. Resources: N/A. Data Curation: CL. Writing original draft: CL, WLS, JSS, AKB. Writing review and editing: CL, JSS, AKB, WLS. Visualization: CL. Supervision: CL. Project administration: CL. Funding acquisition: CL, JSS, AKB, WLS.

Funding. This study was supported by the National Institute on Drug Abuse (NIDA), National Institutes of Health (NIH) under grant 1R01DA060744, part of the BRAIN Initiative (CL, JSS, AKB, WLS).

Declaration of Competing Interests. The authors declare that no competing interests exist. The funders had no role in study design, data collection and analysis, decision to publish, or preparation of the manuscript.

References

Appelhoff, S., M. Sanderson, T.L. Brooks, M. van Vliet, R. Quentin, C. Holdgraf, M. Chaumon, E. Mikulan, K. Tavabi, R. Höchenberger, et al. 2019. Mne-bids: Organizing electrophysiological data into the bids format and facilitating their analysis. *Journal of Open Source Software 4*(44) .

Buzsáki, G. 2006. *Rhythms of the Brain*. Oxford university press.

Calvo, R., C. Martorell, G.B. Morales, S. Di Santo, and M.A. Muñoz. 2024. Frequency-dependent covariance reveals critical spatiotemporal patterns of synchronized activity in the human brain. *Physical Review Letters 133*(20): 208401 .

Choi, B. and T.M. Cover. 1984. An information-theoretic proof of burg's maximum entropy spectrum. *Proceedings of the IEEE 72*(8): 1094–1096 .

Clawson, W.P., N.C. Wright, R. Wessel, and W.L. Shew. 2017. Adaptation towards scale-free dynamics improves cortical stimulus discrimination at the cost of reduced detection. *PLoS computational biology 13*(5): e1005574 .

Cohen, J. 2013. *Statistical power analysis for the behavioral sciences*. Routledge.

Cohen, M.X. 2014. *Analyzing neural time series data: theory and practice*. MIT press.

Dahmen, D., S. Grün, M. Diesmann, and M. Helias. 2019. Second type of criticality in the brain uncovers rich multiple-neuron dynamics. *Proceedings of the National Academy of Sciences 116*(26): 13051–13060 .

Ezaki, T., E.F.d. Reis, T. Watanabe, M. Sakaki, and N. Masuda. 2020. Closer to critical resting-state neural dynamics in individuals with higher fluid intelligence. *Communications Biology 3*(1): 52. https://doi.org/10.1038/s42003-020-0774-y .

Fagerholm, E.D., R. Lorenz, G. Scott, M. Dinov, P.J. Hellyer, N. Mirzaei, C. Leeson, D.W. Carmichael, D.J. Sharp, W.L. Shew, and R. Leech. 2015. Cascades and cognitive state: Focused attention incurs subcritical dynamics. *The Journal of Neuroscience 35*(11): 4626–4634. https://doi.org/10.1523/jneurosci.3694-14.2015 .

Fontenele, A.J., J.S. Sooter, V.K. Norman, S.H. Gautam, and W.L. Shew. 2024. Low-dimensional criticality embedded in high-dimensional awake brain dynamics. *Science Advances 10*(17): eadj9303 .

Fontenele, A.J., J.S. Sooter, E. Ziarati, A. Barreiro, C. Ly, and W. Shew. 2026. Is critical brain dynamics more prevalent than previously thought? *Communications Physics (revised, resubmitted)*: 2025–01. https://doi.org/10.1101/2025.09.02.673722 .

Fuscà, M., F. Siebenhühner, S.H. Wang, V. Myrov, G. Arnulfo, L. Nobili, J.M. Palva, and S. Palva. 2023. Brain criticality predicts individual levels of inter-areal synchronization in human electrophysiological data. *Nature Communications 14*(1): 4736. https://doi.org/10.1038/s41467-023-40056-9 .

Gautam, S.H., T.T. Hoang, K. McClanahan, S.K. Grady, and W.L. Shew. 2015. Maximizing sensory dynamic range by tuning the cortical state to criticality. *PLoS Computational Biology 11*(12): e1004576 .

George, J.S., J. Strunk, R. Mak-McCully, M. Houser, H. Poizner, and A.R. Aron. 2013. Dopaminergic therapy in parkinson's disease decreases cortical beta band coherence in the resting state and increases cortical beta band power during executive control. *NeuroImage: Clinical* 3: 261–270 .

Ghassemkhani, K., K.S. Saroka, and B.T. Dotta. 2025. Evaluating eeg complexity and spectral signatures in alzheimer's disease and frontotemporal dementia: evidence for rostrocaudal asymmetry. *npj Aging 11*(1): 50 .

Gu, C., C.P. Coomans, K. Hu, F.A. Scheer, H.E. Stanley, and J.H. Meijer. 2015. Lack of exercise leads to significant and reversible loss of scale invariance in both aged and young mice. *Proceedings of the National Academy of Sciences 112*(8): 2320–2324 .

Hardstone, R., S.S. Poil, G. Schiavone, R. Jansen, V.V. Nikulin, H.D. Mansvelder, and K. Linkenkaer-Hansen. 2012. Detrended fluctuation analysis: A scale-free view on neuronal oscillations. *Frontiers in Physiology* 3: 450. https://doi.org/10.3389/fphys.2012.00450 .

Hengen, K.B. and W.L. Shew. 2025. Is criticality a unified setpoint of brain function? *Neuron* 113: 1–17. https://doi.org/10.1016/j.neuron.2025.05.020 .

Hohlefeld, F., F. Ehlen, H. Tiedt, L. Krugel, A. Horn, A. Kühn, G. Curio, F. Klostermann, and V.V. Nikulin. 2015. Correlation between cortical and subcortical neural dynamics on multiple time scales in parkinson's disease. *Neuroscience* 298: 145–160 .

Hohlefeld, F., J. Huebl, C. Huchzermeyer, G.H. Schneider, T. Schönecker, A. Kühn, G. Curio, and V.V. Nikulin. 2012. Long-range temporal correlations in the subthalamic nucleus of patients with parkinson's disease. *European Journal of Neuroscience 36*(6): 2812–2821 .

Hu, Y. and H. Sompolinsky. 2022. The spectrum of covariance matrices of randomly connected recurrent neuronal networks with linear dynamics. *PLoS computational biology 18*(7): e1010327 .

Irrmischer, M., S.S. Poil, H.D. Mansvelder, F.S. Intra, and K. Linkenkaer-Hansen. 2018. Strong long-range temporal correlations of beta/gamma oscillations are associated with poor sustained visual attention performance. *European Journal of Neuroscience 48*(8): 2674–2683 .

Jackson, N., S.R. Cole, B. Voytek, and N.C. Swann. 2019. Characteristics of waveform shape in parkinson's disease detected with scalp electroencephalography. *eNeuro 6*(3) .

Kinouchi, O. and M. Copelli. 2006. Optimal dynamical range of excitable networks at criticality. *Nature Physics 2*(5): 348–351. https://doi.org/10.1038/nphys289. q-bio/0601037 .

Lee, C.H., C.H. Juan, H.H. Chen, J.P. Hong, T.W. Liao, I. French, Y.S. Lo, Y.R. Wang, M.L. Cheng, H.C. Wu, et al. 2024. Long-range temporal correlations in electroencephalography for parkinson's disease progression. *Movement Disorders*. https://doi.org/10.1002/mds.30074 .

Li, S. and X.J. Wang. 2022. Hierarchical timescales in the neocortex: Mathematical mechanism and biological insights. *Proceedings of the National Academy of Sciences 119*(6): e2110274119 .

Linkenkaer-Hansen, K., S. Monto, H. Rytsälä, K. Suominen, E. Isometsä, and S. Kähkönen. 2005. Breakdown of long-range temporal correlations in theta oscillations in patients with major depressive disorder. *Journal of Neuroscience 25*(44): 10131–10137 .

Linkenkaer-Hansen, K., V.V. Nikouline, J.M. Palva, and R.J. Ilmoniemi. 2001. Long-range temporal correlations and scaling behavior in human brain oscillations. *Journal of Neuroscience 21*(4): 1370–1377 .

McGregor, J.N., C.A. Farris, S. Ensley, A. Schneider, L.J. Fosque, C. Wang, E.I. Tilden, Y. Liu, J. Tu, H. Elmore, K.D. Ronayne, R. Wessel, E.L. Dyer, K. Bhaskaran-Nair, D.M. Holtzman, and K.B. Hengen. 2024. Failure in a population: Tauopathy disrupts homeostatic set-points in emergent dynamics despite stability in the constituent neurons. *Neuron 112*(21): 3567–3584.e5. https://doi.org/10.1016/j.neuron.2024.08.006 .

Montez, T., S.S. Poil, B.F. Jones, I. Manshanden, J.P.A. Verbunt, B.W.v. Dijk, A.B. Brussaard, A.v. Ooyen, C.J. Stam, P. Scheltens, and K. Linkenkaer-Hansen. 2009. Altered temporal correlations in parietal alpha and prefrontal theta oscillations in early-stage alzheimer disease. *Proceedings of the National Academy of Sciences 106*(5): 1614–1619. https://doi.org/10.1073/pnas.0811699106 .

Morales, G.B., S. Di Santo, and M.A. Muñoz. 2023. Quasiuniversal scaling in mouse-brain neuronal activity stems from edge-of-instability critical dynamics. *Proceedings of the National Academy of Sciences 120*(9): e2208998120 .

Moran, J.K., G. Michail, A. Heinz, J. Keil, and D. Senkowski. 2019. Long-range temporal correlations in resting state beta oscillations are reduced in schizophrenia. *Frontiers in Psychiatry* 10: 517. https://doi.org/10.3389/fpsyt.2019.00517 .

Müller, P.M. and C. Meisel. 2023. Spatial and temporal correlations in human cortex are inherently linked and predicted by functional hierarchy, vigilance state as well as antiepileptic drug load. *PLOS Computational Biology 19*(3): e1010919. https://doi.org/10.1371/journal.pcbi.1010919 .

Müller, P.M., G. Miron, M. Holtkamp, and C. Meisel. 2025. Critical dynamics predicts cognitive performance and provides a common framework for heterogeneous mechanisms impacting cognition. *Proceedings of the National Academy of Sciences 122*(14): e2417117122. https://doi.org/10.1073/pnas.2417117122 .

Newson, J.J. and T.C. Thiagarajan. 2019. Eeg frequency bands in psychiatric disorders: a review of resting state studies. *Frontiers in human neuroscience* 12: 521 .

Nikulin, V.V., E.G. Jönsson, and T. Brismar. 2012. Attenuation of long-range temporal correlations in the amplitude dynamics of alpha and beta neuronal oscillations in patients with schizophrenia. *NeuroImage 61*(1): 162–169. https://doi.org/10.1016/j.neuroimage.2012.03.008 .

O'Byrne, J. and K. Jerbi. 2022. How critical is brain criticality? *Trends in Neurosciences 45*(11): 820–837 .

Pachitariu, M., L. Zhong, A. Gracias, A. Minisi, C. Lopez, and C. Stringer. 2025. A critical initialization for biological neural networks. *bioRxiv*: 2025.01.10.632397. https://doi.org/10.1101/2025.01.10.632397 .

Palva, S. and J.M. Palva. 2018. Roles of brain criticality and multiscale oscillations in temporal predictions for sensorimotor processing. *Trends in Neurosciences 41*(10): 729–743. https://doi.org/10.1016/j.tins.2018.08.008 .

Peng, C.K., S.V. Buldyrev, S. Havlin, M. Simons, H.E. Stanley, and A.L. Goldberger. 1994. Mosaic organization of dna nucleotides. *Physical review e 49*(2): 1685 .

Pernet, C.R., S. Appelhoff, K.J. Gorgolewski, G. Flandin, C. Phillips, A. Delorme, and R. Oostenveld. 2019. Eeg-bids, an extension to the brain imaging data structure for electroencephalography. *Scientific data 6*(1): 103 .

Rockhill, A.P., N. Jackson, J. George, A. Aron, and N.C. Swann. 2021. Uc san diego resting state eeg data from patients with parkinson's disease. *OpenNeuro*. https://doi.org/10.18112/openneuro.ds002778.v1.0.5 .

Safavi, S., M. Chalk, N.K. Logothetis, and A. Levina. 2024. Signatures of criticality in efficient coding networks. *Proceedings of the National Academy of Sciences 121*(41): e2302730121. https://doi.org/10.1073/pnas.2302730121 .

Shew, W.L. and D. Plenz. 2013. The functional benefits of criticality in the cortex. *The neuroscientist 19*(1): 88–100 .

Shew, W.L., H. Yang, T. Petermann, R. Roy, and D. Plenz. 2009. Neuronal avalanches imply maximum dynamic range in cortical networks at criticality. *Journal of neuroscience 29*(49): 15595–15600 .

Siegle, J.H., X. Jia, S. Durand, S. Gale, C. Bennett, N. Graddis, G. Heller, T.K. Ramirez, H. Choi, J.A. Luviano, et al. 2021. Survey of spiking in the mouse visual system reveals functional hierarchy. *Nature 592*(7852): 86–92 .

Sooter, J., A. Fontenele, A. Barreiro, C. Ly, K. Hengen, and W. Shew. 2026. Defining and measuring proximity to criticality. *Proceedings of the National Academy of Sciences (revised, resubmitted)*: 1–27. https://doi.org/10.1101/2025.08.03.668332 .

Swann, N.C., C. De Hemptinne, A.R. Aron, J.L. Ostrem, R.T. Knight, and P.A. Starr. 2015. Elevated synchrony in p arkinson disease detected with electroencephalography. *Annals of neurology 78*(5): 742–750 .

Tcheslavski, G. 2025. Eeg bdf reader. https://www.mathworks.com/matlabcentral/fileexchange/13070-eeg-bdf-reader. MATLAB Central File Exchange; Accessed October 2, 2024.

Tian, Y., Z. Tan, H. Hou, G. Li, A. Cheng, Y. Qiu, K. Weng, C. Chen, and P. Sun. 2022. Theoretical foundations of studying criticality in the brain. *Network Neuroscience 6*(4): 1148–1185 .

Tomczak, M. and E. Tomczak. 2014. The need to report effect size estimates revisited. an overview of some recommended measures of effect size. *Trends in sports sciences* 21 .

van Meegen, A. and S.J. van Albada. 2021. Microscopic theory of intrinsic timescales in spiking neural networks. *Physical Review Research 3*(4): 043077 .

Wei, Y., C. Zhang, Y. Peng, C. Chen, S. Han, W. Wang, Y. Zhang, H. Lu, and J. Cheng. 2024. Mri assessment of intrinsic neural timescale and gray matter volume in parkinson's disease. *Journal of Magnetic Resonance Imaging 59*(3): 987–995 .

Xin, Y., Y. Cui, S. Yu, and N. Liu. 2025. Genetic contributions to brain criticality and its relationship with human cognitive functions. *Proceedings of the National Academy of Sciences 122*(26): e2417010122. https://doi.org/10.1073/pnas.2417010122 .

Zeraati, R., T.A. Engel, and A. Levina. 2022. A flexible bayesian framework for unbiased estimation of timescales. *Nature computational science 2*(3): 193–204 .

Zeraati, R., A. Levina, J.H. Macke, and R. Gao. 2024. Neural timescales from a computational perspective. *arXiv preprint arXiv:2409.02684* .

Zimmern, V. 2020. Why brain criticality is clinically relevant: A scoping review. *Frontiers in Neural Circuits* 14: 54. https://doi.org/10.3389/fncir.2020.00054 .